Constraints on Density and Shear Velocity Contrasts at the Inner Core Boundary

Aimin Cao and Barbara Romanowicz

Seismological Laboratory, University of California, Berkeley

January 8, 2004

(Fast-track paper is requested)

Short title: Density and Shear Velocity Contrasts at ICB

Corresponding author: Barbara Romanowicz

ph: 510-642-1844, fax: 510-643-5811, email: barbara@seismo.berkeley.edu

Abstract

The density jump ($\Delta\rho_{ICB}$) at the Inner Core Boundary (ICB) is an important constraint on the dynamics and history of the earth's core. Two types of seismological data sensitive to $\Delta\rho_{ICB}$ have been studied since the 1970's: free oscillation eigenfrequencies and amplitudes of core reflected phases (PKiKP/PcP). The reference PREM model (Dziewonski and Anderson, 1981), based largely on normal mode data, has a relatively low value of $\Delta\rho_{ICB} = 0.60 gcm^{-3}$, whereas most studies based on PKiKP/PcP amplitude ratios find significantly larger values, sometimes in excess of $1.0 gcm^{-3}$. It has been argued that, because PKiKP is rarely observed in the distance range considered ($10 - 70^o$), the latter type of measurement provides only upper bounds on $\Delta\rho_{ICB}$ (e.g. Shearer and Masters, 1990). We have analyzed 10 years of high quality global broadband data accumulated since the work of Shearer and Masters (1990). We systematically analyzed over 4500 seismograms from intermediate/deep events (depth > 70 km) and nuclear explosions, in the distance range $10 - 70^o$. The data were filtered in the band-pass 0.7-3 Hz. We performed a rigorous data selection and identified 5 pairs of very clear (Quality A), and 15 possible (Quality A^-) PKiKP and PcP arrivals. In addition, 58 records showed no PKiKP but a clear PcP. Together, we obtain a much less dispersed dataset than previously available, with the quality A data at the lower end of the ensemble of amplitude ratios versus distance. We combine our high quality measurements with 2 measurements from the literature that fall within our rigorous selection criteria and obtain estimates of $\Delta\rho_{ICB}$ in the range $0.6 - 0.9 gcm^{-3}$ and $\Delta\beta_{ICB}$ in the range $2 - 3 kms^{-1}$. Our estimate of $\Delta\rho_{ICB}$ is in agreement with a recent reevaluation of normal mode data (Masters and Gubbins, 2004), thus reconciling results from body wave and mode studies and providing a tighter constraint on $\Delta\rho_{ICB}$ for geodynamicists. Our study also provides evidence for a shear velocity gradient at the top of the inner core.

Key words: ICB, inner core, density contrast, S-velocity contrast, PKiKP/PcP amplitude ratio.

1 Introduction

The density $\Delta\rho_{ICB}$ and shear velocity $\Delta\beta_{ICB}$ contrasts at the Inner Core Boundary (ICB), estimated using seismological methods, are important constraints for the understanding of the character of the Earth's geodynamo and the evolution of the inner core (e.g. Hewitt *et al.*, 1975; Gubbins, 1977; Buffett *et al.*, 1996; Stacey and Stacey, 1999).

So far, three distinct approaches have been used to constrain the density and shear velocity contrasts at the ICB, but the resulting estimates vary significantly. The first method uses data for normal modes which are sensitive to the inner core structure (Gilbert *et al.*, 1973; Gilbert and Dziewonski, 1975; Masters, 1979). The reference PREM model (Dziewonski and Anderson, 1981), which incorporates constraints from normal mode data, has $\Delta\rho_{ICB} = 0.60 gcm^{-3}$ and $\Delta\beta_{ICB} = 3.5 kms^{-1}$.

The second method uses body wave amplitude and waveform modeling of PKP and PKiKP. This technique has resulted in estimates of $\Delta\rho_{ICB} \sim 0 - 1.2 gcm^{-3}$ (Häge, 1983) and $\Delta\beta_{ICB}$ ranging from $\sim 0 kms^{-1}$ (Choy and Cormier, 1983), to $2.5 - 3.0 kms^{-1}$ (Häge, 1983), or $2 - 4 kms^{-1}$ (Cummins and Johnson, 1988).

The third method is based on measurements of $PKiKP/PcP$ amplitude ratios in the distance range 10^o to 70^o. The first convincing observation of PKiKP in this distance range was reported by Engdahl *et al.* (1970) and was based on stacking of LASA array data. Bolt and Qamar (1970) first proposed the amplitude ratio technique and estimated a maximum density jump of 1.8 gcm^{-3} at the ICB. Souriau and Souriau (1989) further constrained the density jump to be in the range of 1.35-1.6 gcm^{-3},

based on array data. Finally, Shearer and Masters (1990) estimated maximum bounds on PKiKP/PcP ratios and obtained $\Delta\rho_{ICB} < 1.0 gcm^{-3}$ and $\Delta\beta_{ICB} > 2.5 kms^{-1}$.

Compared with the results derived from normal modes, the constraint on the density contrast from body waves is considered to be much less robust, as it is based on few reliable measurements, and most recently, a set of rather scattered "upper bound" data (Shearer and Masters, 1990). Indeed, PKiKP is such a weak phase in the distance range from 10^o to 70^o that it is rarely observed, and even more rarely so, without stacking. Shearer and Masters (1990) systematically searched for PKiKP arrivals in over 4900 GDSN vertical component seismograms. They found only two seismograms with both clear PKiKP and clear PcP arrivals. Both Souriau and Souriau (1989) and Shearer and Masters (1990) used "non-observations" of PKiKP as upper bounds on the observed amplitude of this phase, leading to upper bounds on the corresponding PKiKP/PcP amplitude ratios.

At present, geodynamo simulations usually refer to the density contrast derived from normal mode data. Nevertheless, a recent geodynamo study (Stacey and Stacey, 1999) explicitly pointed out that the inner core would not have existed 2 billion years ago if the density contrast at the ICB was as low as inferred from current seismological models. This is obviously against the paleomagnetic evidence, which shows that the Earth has sustained a magnetic field for at least 3 billion years (McElhinny and Senanayake, 1980).

In this study, we take advantage of the accumulation of large quantities of high quality global broadband seismic data in the last 15 years, to revisit the question

of estimating the density and shear velocity contrasts at the ICB using PKiKP/PcP amplitude ratios.

2 Data, Method, and Results

All of the broadband vertical component data for deeper ($\geq 70km$) natural earthquakes and nuclear explosions in the distance range 10^o to 70^o, for the time span 1990-1999, were systematically downloaded from IRIS Data Management Center (DMC), to search for simultaneous observations of PKiKP and PcP. The ray paths of these phases for a given source-station pair are shown in Fig. 1. The seismograms were filtered in the band pass 0.7-3 Hz (the dominant frequency of PKiKP is typically ~ 1 Hz). We used relocated origin time and hypocentral parameters from the catalog of Engdahl *et al.* (1998), recently extended to include the year 1999. We then marked the seismograms with the theoretical arrival times of 11 phases (PcP, PKiKP as well as P, pP, sP, PP, PPP, S, sS, SS, and ScS) computed with respect to model $AK135$ (Kennett *et al.*, 1995), and corrected for ellipticity (Dziewonski and Gilbert, 1976). Those 9 phases are the most likely ones to interfere with our target PcP and PKiKP phases. Finally only the seismograms were kept whose background noise before the direct P wave was significantly less than the average amplitude level in the vicinity of the theoretical PKiKP arrival.

We divided the resulting 79 seismograms (out of an initial collection of more than 4500) into three categories (A, A^-, B), according to the following criteria. Quality A data exhibit very clear PKiKP and PcP phases within 5 seconds of their expected

theoretical arrivals, there is no other theoretical arrival 15 seconds preceding or following the identified PKiKP or PcP phases (unless the potential interfering arrival can be verified from a nodal plane inspection), and the average peak-to-peak noise-to-signal ratio is less than 40%. Quality A^- includes seismograms with clear PKiKP and PcP phases within 5 seconds of their theoretical arrivals, there is no other theoretical arrival 15 seconds preceding or following the identified PKiKP or PcP, but the average peak-to-peak noise-to-signal ratio is larger than 40%. Finally, in Quality B, we collected seismograms with no observable PKiKP phase within 5 seconds of its theoretical arrival, but there is also no other predicted arrival 50 seconds preceding and 10 seconds following the theoretical PKiKP arrival, and the PcP phase is very clear and within 5 seconds of its predicted arrival.

Based on the above criteria, we collected 5, 15, and 59 Quality A, A^-, and B data, respectively. All of our Quality A data are shown in Fig. 2. We measured peak-to-peak amplitudes of the identified PKiKP and PcP phases and computed PKiKP/PcP amplitude ratios for Quality A and Quality A^- data. For Quality B data, the maximum peak-to-peak amplitude 5 seconds around the PKiKP theoretical arrival was used as an upper limit for the PKiKP amplitude (e.g. Shearer and Masters, 1990). In the epicentral distance range considered, for Quality A data, the difference in take-off angles between PKiKP and PcP is small (approximately from 2.3^o to 11.9^o) and the two rays are close to the maxima of the radiation lobes, as we have verified (Figure 2), Therefore, the effect of the radiation pattern at the source is neglected (e.g. Souriau and Souriau, 1989).

Additionally, we also applied our selection criteria to re-examine available seismograms from the literature. Shearer and Masters (1990) identified only two seismograms with clear simultaneous PKiKP and PcP observations. The theoretical SS arrival is only 1.97 seconds in front of the theoretical PKiKP arrival for the first seismogram. For their second seismogram, a theoretical SS arrival is 13.38 seconds in front of the theoretical PKiKP arrival with reference to model $AK135$. Hence it is possible that the discrepancy in the corresponding PKiKP/PcP amplitude ratios (almost a factor of 3) is due to interference with SS in the first example, even though the corresponding epicentral distances are almost the same (39.8^o and 39.2^o, respectively). We included the second of these two measurements, which, according to our criteria, is much more reliable, in our Quality A dataset. We also included one stacking measurement ($0.032, \Delta = 51.4^o$) (Schweitzer, 1992), which has recently been re-measured ($0.038 - 0.048$) by the author himself (Schweitzer, personal communication, 2003).

We then compared our PKiKP/PcP amplitude ratio measurements to theoretical predictions using several reference models: PREM (Dziewonski and Anderson, 1981) , PREM2 (Song and Helmberger, 1995), IASP91 (Kennett and Engdahl, 1991), and AK135 (Kennett *et al.,* 1995). Models differ by the velocity contrasts and density contrasts at the ICB and CMB (Table 1).

Table 1. Comparison of seismic contrasts at ICB and CMB in the four models

Models	$\Delta\alpha_{ICB}$	$\Delta\alpha_{CMB}$	$\Delta\beta_{ICB}$	$\Delta\beta_{CMB}$	$\Delta\rho_{ICB}$	$\Delta\rho_{CMB}$
PREM	0.67	5.65	3.50	7.26	0.60	4.34
PREM2	0.78	5.45	3.50	7.26	0.60	4.34
IASP91	0.83	5.68	3.44	7.30	0.56	4.36
AK135	0.75	5.66	3.50	7.28	0.56	4.36

** units of velocity and density contrasts are kms^{-1} and gcm^{-3}, respectively*

In order to obtain the theoretical PKiKP/PcP amplitude ratio, we calculated transmission and reflection coefficients at various seismic discontinuities as well as ratios of PKiKP and PcP geometrical spreading factors, which may be readily expressed as functions of ray parameters and their corresponding derivatives (Bolt and Qamar, 1970). As for the attenuation factor, we neglected its effect on the predicted ratios in the mantle due to the arguably close ray paths of PKiKP/PcP there, and we assumed that the quality factor in the outer core is infinite because there is no significant change when using a realistic quality factor ($\geq 10,000$) (Cormier and Richards, 1976). As previous authors, we also neglected finite frequency effects, as these are likely within the uncertainties of other factors such as the earth models used, in particular, a possible topography of the CMB. When we explored different models, the computed geometrical spreading factors were very close, but reflection coefficients varied significantly. For each of the models, we searched for the best variance reduction in the parameter space $(\Delta\rho_{ICB}, \Delta\beta_{ICB})$. We note that the set of Quality A measurements spans the entire epicentral distance range considered (Fig. 3), thus

providing relatively tight fits on the resulting ICB parameters: $\Delta\beta_{ICB}$ is constrained at large distance ($\Delta > 50^o$) whereas $\Delta\rho_{ICB}$ is constrained by data at shorter distance. The best fitting density contrasts at the ICB vary somewhat from one model to the other, as illustrated in Fig. 4: from $\sim 0.6 gcm^{-3}$ (IASP91) to $\sim 0.9 gcm^{-3}$ (PREM2). On the other hand, the range of the best fitting shear velocity contrasts is somewhat tighter: from $\sim 2.4 kms^{-1}$ to $\sim 2.6 km^{-1}$. In fact, because the shear velocity and density contrasts at the CMB are very consistent in each model, the uncertainty in $\Delta\rho_{ICB}$ and $\Delta\beta_{ICB}$ stems mostly from the difference in $\Delta\alpha_{ICB}$ and $\Delta\alpha_{CMB}$ for the different models. In particular, the results for IASP91 show the lowest $\Delta\rho_{ICB}$ because its $\Delta\alpha_{ICB}$ is significantly larger ($> 6\%$) than for the other models.

3 Discussion

In our study, we have identified 7 definite PKiKP arrivals and 15 probable ones, but compared with the huge initial data pool, the percentage of observations is still quite small. It has been argued that PKiKP is observable only when it is anomalously large, probably due to focusing from heterogeneities within the Earth, and even the PKiKP/PcP data measured from the identified PKiKP arrivals represent only upper limits for this ratio (Souriau and Souriau, 1989; Shearer and Masters, 1990). However, when we compare our A, A^- and B quality measurements (Fig. 3), we note the following: 1) the data are overall much less scattered than in previous studies; 2) the A quality measurements generally fall near the lower bound of all our measurements, including those found in the literature and corresponding to explicit reports of

PKiKP observations. We thus believe that, although the PKiKP arrival is generally weak, our Quality A observations are not significantly biased either by interfering phases (we ruled those out) or focusing effects, and that they simply correspond to favorable geometry with respect to the maximum in P radiation pattern, as we have checked. On the other hand, some of our A^- measurements plot above the best fitting theoretical curves computed using only the quality A data, which indicates that, for these measurements, there may be some constructive interference between noise and PKiKP. We did not use these data in computing the optimal ICB parameters, but we find that they are compatible with the resulting predictions, as are our Quality B data (Fig. 3).

On the other hand, we did not include other data from the literature for which seismograms were not available for verification (we show them as open symbols in Fig. 3.). In particular, several previous measurements used stacking of traces (e.g. Bolt and Qamar, 1970; Souriau and Souriau, 1989). The stacking technique is very effective in extracting the weak seismic signal, but it seems difficult to keep the amplitudes of PKiKP and PcP arrivals from being distorted in the summation (especially when using a nonlinear stacking process).

The density contrast inferred at the ICB depends on the reference seismic models (Fig. 4). The main reason is that the reflection coefficients of PcP at the CMB and PKiKP at the ICB also depend on the corresponding P-wave velocity contrasts. In general, the larger $\Delta\alpha_{ICB}$, the lower $\Delta\rho_{ICB}$, for a fixed $\Delta\alpha_{CMB}$; the larger $\Delta\alpha_{CMB}$, the lower $\Delta\rho_{ICB}$, for a fixed $\Delta\alpha_{ICB}$. Further refinement of $\Delta\rho_{ICB}$ will depend on

the improvement of our knowledge of P-wave velocity structure at both ICB and CMB. In the four reference seismic models, PREM (Dziewonski and Anderson, 1981) and IASP91 (Kennett and Engdahl, 1991) are based on absolute travel times from the International Seismological Center (ISC) and free oscillation eigenfrequencies. PREM2 (Song and Helmberger, 1995) is modified from PREM by fitting PKP differential travel times, amplitude ratios, and waveforms, but shear velocity and density structure in PREM are left untouched. AK135 (Kennett *et al.,* 1995) is updated from IASP91 by the authors themselves taking additional account of PKP differential travel times and event relocations. The differences in velocity between AK135 and IASP91 are generally very small except for the reduced velocity gradients at the ICB in AK135. From our experience (Tkalčić *et al.,* 2002) AK135 gives better fits to PKP travel time data than PREM and IASP91. We are therefore inclined to favor the bounds obtained from AK135. The main difference between PREM and IASP91 is in the $\Delta\alpha_{ICB}$; and the main difference between PREM2 and AK135 is in $\Delta\alpha_{CMB}$ (Table 1). We note from Fig. 3 and 4 that the PREM $\Delta\rho_{ICB} = 0.6gcm^{-3}$ is clearly a minimum value compatible with the data, and that $\Delta\rho \approx 0.85gcm^{-3}$ is optimal.

Compared with the constraint on $\Delta\rho_{ICB}$, the constraint on $\Delta\beta_{ICB}$ (2-3 kms^{-1}) is almost independent of the seismic models. While compatible with the results of other body wave studies, this well-constrained value is significantly lower than the average shear velocity contrast ($\sim 3.5km^{-1}$) estimated from normal mode data. It is constrained by the trend in PKiKP/PcP amplitude ratios at distances $\Delta > 50^o$ (Fig. 3). This may provide further evidence for the existence of a shear velocity gradient

at the top of the inner core (e.g. Choy and Cormier, 1983; Häge, 1983; Cummins and Johnson, 1988). Indeed, normal mode data provide an estimate averaged over tens of km of depth, whereas the reflected wave data considered here provide a much more local estimate.

In the quality A observations, which we used to constrain density and shear velocity contrasts at the ICB, all of the corresponding focal depths of the natural events are deeper than 100 km. The usually shorter source time functions than those of shallow ($< 70km$) events (with equivalent magnitudes) enhance the sharpness and signal-to-noise ratio of the phase arrivals. This beneficial feature may significantly help us to uniquely identify the weak PKiKP arrivals. Although our strict selection criteria have limited the global coverage of our observations, the quality A data span a wide geographical distribution (Fig. 5). The PKiKP (PcP) bouncing points at the ICB (also CMB) are located beneath Western Pacific Ocean, Australia, Southeastern Asia, Middle Asia, Eastern Europe, and South America.

4 Conclusions

We have obtained a set of high quality PKiKP and PcP observations in the distance range 10^o to 70^o that provide tighter constraints on the density and shear velocity contrasts at the ICB. The identification of arguably unbiased PKiKP and PcP arrivals greatly improve the body wave constraints on the density and shear velocity contrasts at the ICB. Our preferred value for $\Delta\rho_{ICB}$ is $\sim 0.85 gcm^{-3}$, with some uncertainties remaining, primarily due to uncertainties in the P-wave velocity contrast at the ICB.

Our estimates are compatible with a recent reevaluation ($0.64 - 1.0 gcm^{-3}$) of normal mode data (Masters and Gubbins, 2004), thus reconciling previously incompatible results from normal mode and body wave measurements. On the other hand, the shear velocity contrast at the ICB is somewhat lower than the average shear velocity in the inner core as obtained from normal mode data. Our study thus provides evidence for 1) a larger density contrast at the ICB than generally assumed in dynamo studies and 2) the existence of a gradient of structure at the top of the inner core. The former is of significance for studies of the geodynamo, whose energy is proportional to the assumed density contrast (Stacey and Stacey, 1999). The inferred gradient may also provide constraints on the cooling and solidifying processes in the inner core and may be of significance in studies of the geodynamo, as well as of the chemical and physical evolution of the inner core (e.g. Gubbins, 1977; Loper, 1978,1991; Gubbins *et al.*, 1979).

5 Acknowledgments

This study benefited from enlightening discussion with A. Souriau, P. Shearer and J. Schweitzer. We thank G. Masters for a preprint of his paper with D. Gubbins. We are grateful to the IRIS Data Management Center (DMC) for making waveform data readily acceptable, and to the network or station operators who contributed data to the DMC. This material is based upon work partially supported by the National Science Foundation under Grant No. EAR-0308750, and this is Berkeley Seismological Laboratory contribution 04-01.

6 References

Backus, G.E., 1975. Gross thermodynamics of heat engines in deep interior of Earth, *Nat. Acad. Sci. USA, 72,* 1555-1558.

Bolt, B.A. and Qamar, A., 1970. Upper bound to the density jump at the boundary of the Earth's inner core, *Nature, 228,* 148-150.

Buffett, B.A., Huppert, H.E., Lister, J.R., and Woods, A.W., 1996. On the thermal evolution of the Earth's core, *J. Geophys. Res., 101,* 7989-8006.

Choy, G.L., and Cormier, V.F., 1983. The structure of the inner core inferred from short-period and broadband GDSN data, *Geophys. J. R. astr. Soc.,* 21-29.

Cormier, V.F., and Richards, P.G., 1976. Comments on 'damping of core waves' by A. Qamar and A. Eisenberg, *J. Geophys. Res.,* 81, 3066-3068.

Cummins, P., and Johnson, L.R., 1988. Short-period body wave constraints of properties of the Earth's inner core boundary, *J. Geophys. Res., 93,* 9058-9074.

Dziewonski, A.M., and Gilbert, F., 1976. The effect of small, aspherical perturbations on travel times and a re-examination of the corrections for ellipticity, *Geophys. J. R. Astron. Soc., 44,* 7-17.

Dziewonski, A.M., and Anderson, D.L., 1981. Preliminary Reference Earth Model, *Phys. Earth planet. Inter., 25,* 297-356.

Engdahl, E.R., van der Hilst, R.D., and Buland, R.P., 1998. Global teleseismic earthquake relocation with improved travel times and procedures for depth determination, *Bull. Seism. Soc. Am., 88,* 722-743.

Gilbert, F., Dziewonski, A.M., and Brune, J.N., 1973. An informative solution to

a seismological inverse problem, *Proc. Natl. Acad. Sci., 70,* 1410-1413.

Gilbert, F., and Dziewonski, A.M., 1975. An application of normal mode theory to the retrieval of structural parameters and source mechanisms from seismic spectra. *Phil. Trans. R. Soc. Lond., A278,* 187-269.

Gubbins, D., 1977. Energetics of the Earth's core, *J. Geophys., 43,* 453-464.

Gubbins, D., Masters, T.G., and Jacobs, J.A., 1979. Thermal evolution of the Earth's core, *Geophys. J. R. Astron. Soc., 59,* 57-99.

Häge, H., 1983. Velocity constraints for the inner core inferred from long-period PKP amplitudes, *Phys. Earth Planet. Inter., 31,* 171-185.

Hewitt, J.M., McKenzie, D.P., and Weiss, N.O., 1975. Dissipative heating in convective flows, *J. Fluid Mech., 68,* 721-738.

Kennett, B.L.N.,and Engdahl, E.R., 1991. Traveltimes for global earthquake location and phase identification, *Geophys. J. Int., 105,* 429-465.

Kennett, B.L.N., Engdahl, E.R., and Buland, R., 1995. Constrains on seismic velocities in the Earth from traveltimes, *Geophys. J. Int., 122,* 108-124.

Labrosse, S., Poirier, J.P., and LeMouel, J.L., 1997. On cooling of the Earth's core, *Phys. Earth Planet. Int., 99,* 1-17.

Loper, D.E., 1978. The gravitationally powered dynamo, *Geophys. J. R. Astron. Soc., 54,* 389-404.

Loper, D.E., 1991. The nature and consequences of thermal interactions twixt core and mantle, *G. Geomagn. Geoelectr., 43,* 79-91.

Masters, G., 1979. Observational constraints on the chemical and thermal struc-

ture of the earth's deep interior. *Geophys. J. R. Astron. Soc., 57,* 507-534.

Masters, G., and Gubbins, D., 2004. On the resolution of density within the Earth. *Geophys. J. Int.,* in press.

McElhinny, M.W., and Senanayake, W.E., 1980. Paleomagnetic evidence for the existence of the geomagnetic field 3.5Ga ago, *J. Geophys. Res., 85,* 3523-3528.

Mollett, S., 1984. Thermal and magnetic constraints on the cooling of the Earth, *Geophys. J. R. Astron. Soc., 76,* 653-666.

Shearer, P.M., and Masters, G., 1990. The density and shear velocity contrast at the inner core boundary, *Geophys. J. Int., 102,* 491-498.

Song, X., and Helmberger, D.V., 1995. A P-wave model of the Earth's core, *J. geophys. Res., 100,* 9817-1930.

Souriau, A., and Souriau, M., 1989. Ellipticity and density at the inner core boundary from sub-critical PKiKP and PcP data, *Geophys. J. Int., 98,* 39-54.

Stacey, F.D., and Stacey, C.H.B., 1999. Gravitational energy of core evolution: implications for thermal history and geodynamo power, *Phys. Earth Planet. Int., 110,* 83-93.

Schweitzer, J., 1992. PKikP and PcP observations of the Chinese Nuclear Test on May 21, 1992 05:00 UTC, *Eos. Trans. Am. Geophys. Union,* 408.

Tkalčić, H., Romanowicz, B., and Houy, N., 2002. Constraints on $D"$ structure using PKP(AB-DF), PKP(BC-DF) and PcP-P traveltime data from broad-band records, *Geophys. J. Int., 148,* 599-616.

Figure 1. Ray paths of PKiKP (reflected P wave from the ICB) and PcP (reflected P wave from the CMB). The star denotes an assumed source and the triangle denotes a seismological station.

Figure 2. Quality A observations with very clear PKiKP and PcP phases. Dashed lines are the theoretical arrival times referring to AK135 seismic model, taking into account ellipticity corrections. From top to bottom, the observed PKiKP/PcP amplitude ratios are 0.052, 0.052, 0.071, 0.151, and 0.250, respectively. At right of each pair of traces are the corresponding P-wave radiation patterns derived from the Harvard CMT moment tensors. From top to bottom the differential take-off angles between PKiKP and PcP are approximately 11.9^o, 9.6^o, 10.0^o, 8.6^o, and 2.3^o, respectively. The last observation (SANG) corresponds to a nuclear explosion event.

Figure 3. Measurements of PKiKP/PcP amplitude ratios. The red stars denote the Quality A data, and their error bars are derived from the fractional ratos of the average peak-to-peak amplitudes of background noise to the peak-to-peak amplitude of the identified phase arrivals; the red hexagon is Shearer and Masters' (1990) second measurement with clear PKiKP; the inverted red triangle is a stacking measurement (Schweitzer, 1992) which has been remeasured by the author himself recently; the grey squares denote the Quality A^- data; and the black dots are the Quality B data. The curves are the theoretical PKiKP/PcP amplitude ratio calculated with respect to PREM model. For the dashed green curve $\Delta\rho_{ICB} = 0.60 gcm^{-3}$ and $\Delta\beta_{ICB} = 3.5 kms^{-1}$ (original values in PREM model); for the dashed orange curve $\Delta\rho_{ICB} = 0.60 gcm^{-3}$ and $\Delta\beta_{ICB} = 2.5 kms^{-1}$; for the dashed red curve $\Delta\rho_{ICB} = 0.85 gcm^{-3}$ and

$\Delta\beta_{ICB} = 3.5kms^{-1}$; and for the solid blue curve $\Delta\rho_{ICB} = 0.85gcm^{-3}$ and $\Delta\beta_{ICB} = 2.5kms^{-1}$ (our best fitting values using PREM model). The open symbols are other data from previous studies, which were not used in our analysis (triangles: Souriau and Souriau, 1989; hexagon: Shearer and Masters, 1990; diamonds: Engdahl *et al.*, 1970; Bolt and Qamar, 1970).

Figure 4. Variance reduction with respect to PREM (Dziewonski and Anderson, 1981), PREM2 (Song and Helmberger, 1995), IASP91 (Kennett and Engdahl, 1991), and AK135 (Kennett et al., 1995). The best fitting $\Delta\rho_{ICB}$ and $\Delta\beta_{ICB}are\sim 0.85gcm^{-3}$ and $\sim$2.5 kms^{-1}, $\sim 0.91gcm^{-3}$ and $\sim 2.6kms^{-1}$, $\sim 0.65gcm^{-3}$ and $\sim 2.5kms^{-1}$, and $\sim 0.75gcm^{-3}$ and $\sim 2.4kms^{-1}$, respectively.

Figure 5. Geographical distribution of PKiKP and PcP ray paths. The red, blue, and black lines correspond to Quality A, A^{-}, and B subsets of data, respectively. The stars denote the events and the squares denote the stations.

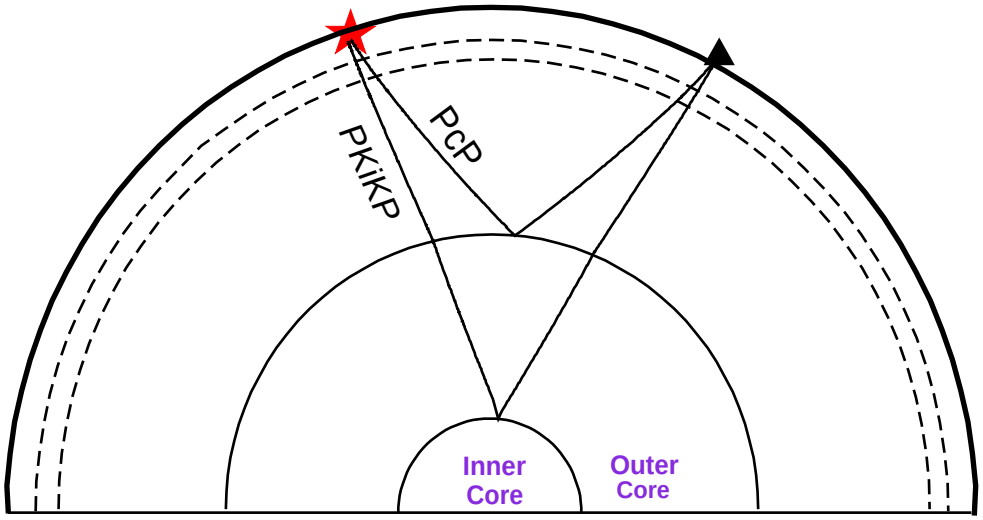

Figure 1: Ray paths of PKiKP (reflected P wave from the ICB) and PcP (reflected P wave from the CMB). The star denotes an assumed source and the triangle denotes a seismological station.

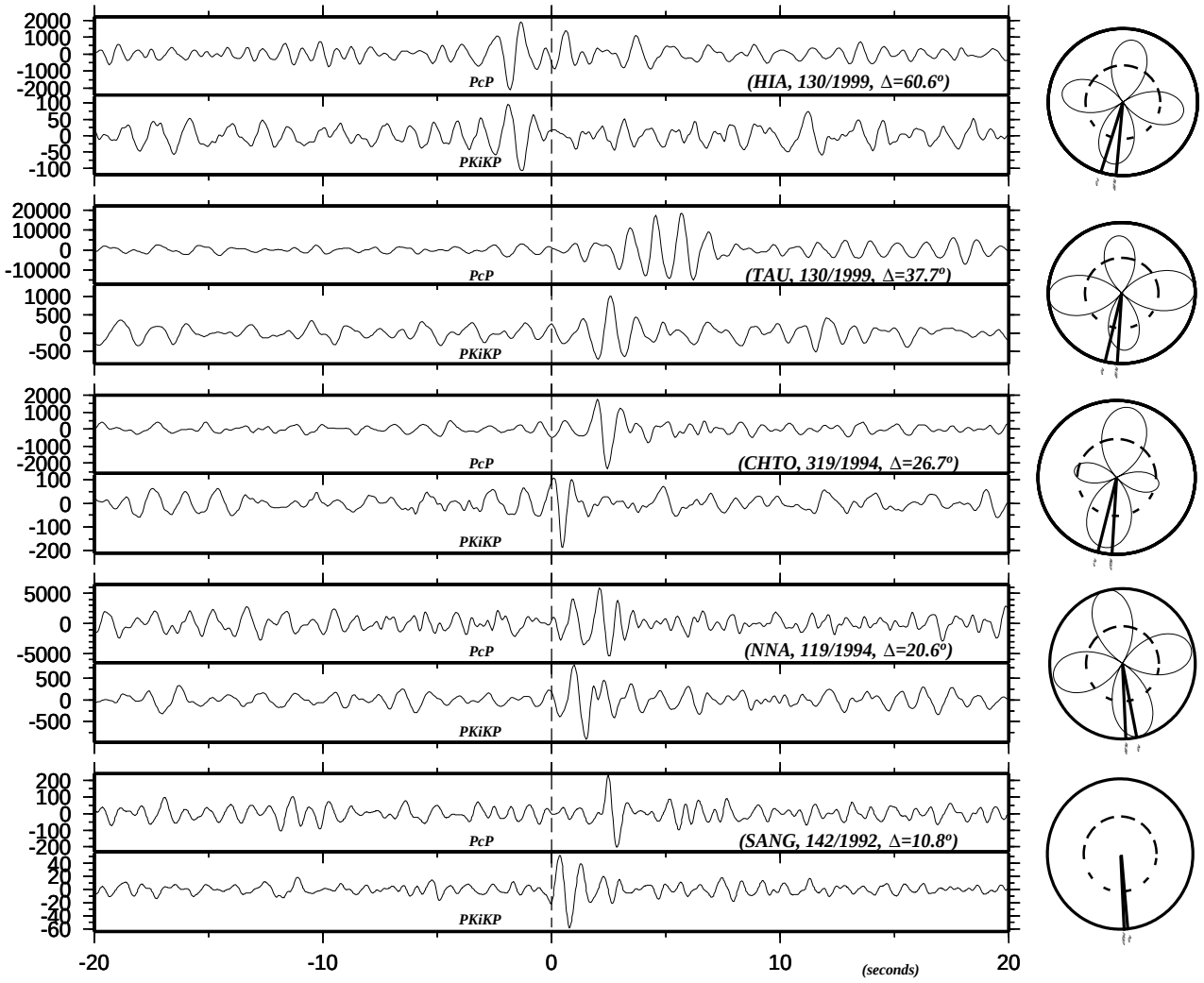

Figure 2: Quality A observations with very clear PKiKP and PcP phases. Dashed lines are the theoretical arrival times referring to AK135 seismic model, taking into account ellipticity corrections. From top to bottom, the observed PKiKP/PcP amplitude ratios are 0.052, 0.052, 0.071, 0.151, and 0.250, respectively. At right of each pair of traces are the corresponding P-wave radiation patterns derived from the Harvard CMT moment tensors. From top to bottom the differential take-off angles between PKiKP and PcP are approximately 11.9^o, 9.6^o, 10.0^o, 8.6^o, and 2.3^o, respectively. The last observation (SANG) corresponds to a nuclear explosion event.

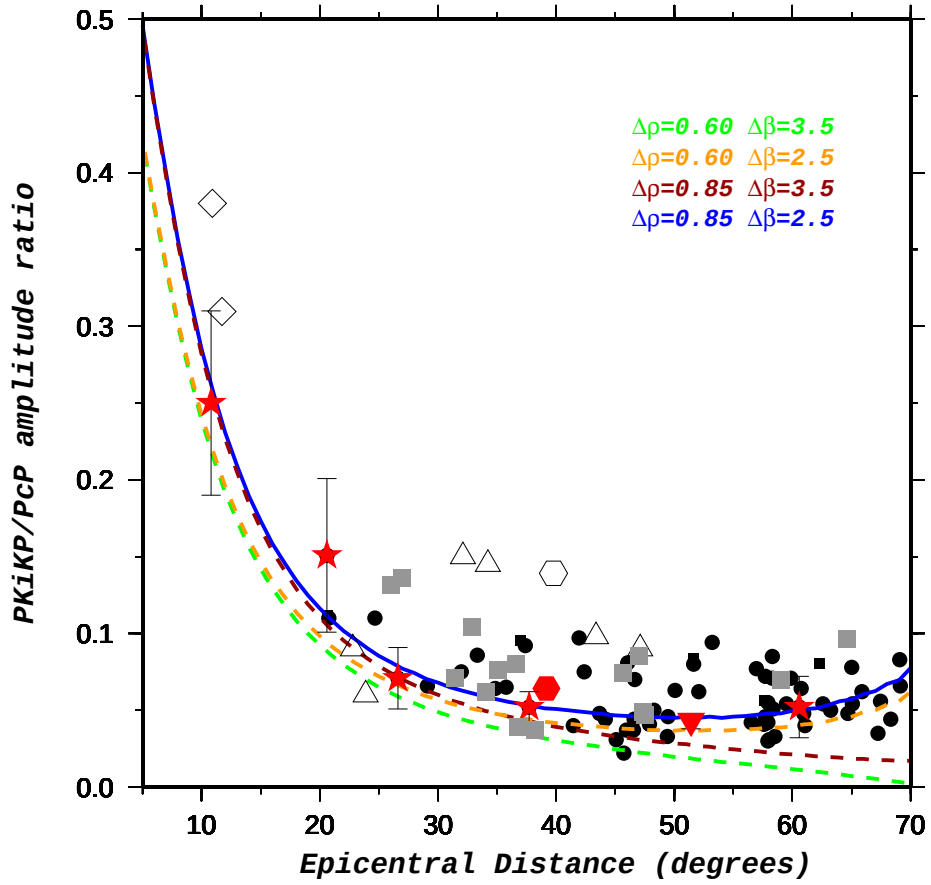

Figure 3: Measurements of PKiKP/PcP amplitude ratios. The red stars denote the Quality A data, and their error bars are derived from the fractional ratos of the average peak-to-peak amplitudes of background noise to the peak-to-peak amplitude of the identified phase arrivals; the red hexagon is Shearer and Masters' (1990) second measurement with clear PKiKP; the inverted red triangle is a stacking measurement (Schweitzer, 1992) which has been remeasured by the author himself recently; the grey squares denote the Quality A^- data; and the black dots are the Quality B data. The curves are the theoretical PKiKP/PcP amplitude ratio calculated with respect to PREM model. For the dashed green curve $\Delta\rho_{ICB} = 0.60 gcm^{-3}$ and $\Delta\beta_{ICB} = 3.5 kms^{-1}$ (original values in PREM model); for the dashed orange curve $\Delta\rho_{ICB} = 0.60 gcm^{-3}$ and $\Delta\beta_{ICB} = 2.5 kms^{-1}$; for the dashed red curve $\Delta\rho_{ICB} = 0.85 gcm^{-3}$ and $\Delta\beta_{ICB} = 3.5 kms^{-1}$; and for the solid blue curve $\Delta\rho_{ICB} = 0.85 gcm^{-3}$ and $\Delta\beta_{ICB} = 2.5 kms^{-1}$ (our best fitting values using PREM model). The open symbols are other data from previous studies, which were not used in our analysis (triangles: Souriau and Souriau, 1989; hexagon: Shearer and Masters, 1990; diamonds: Engdahl *et al.*, 1970; Bolt and Qamar, 1970).

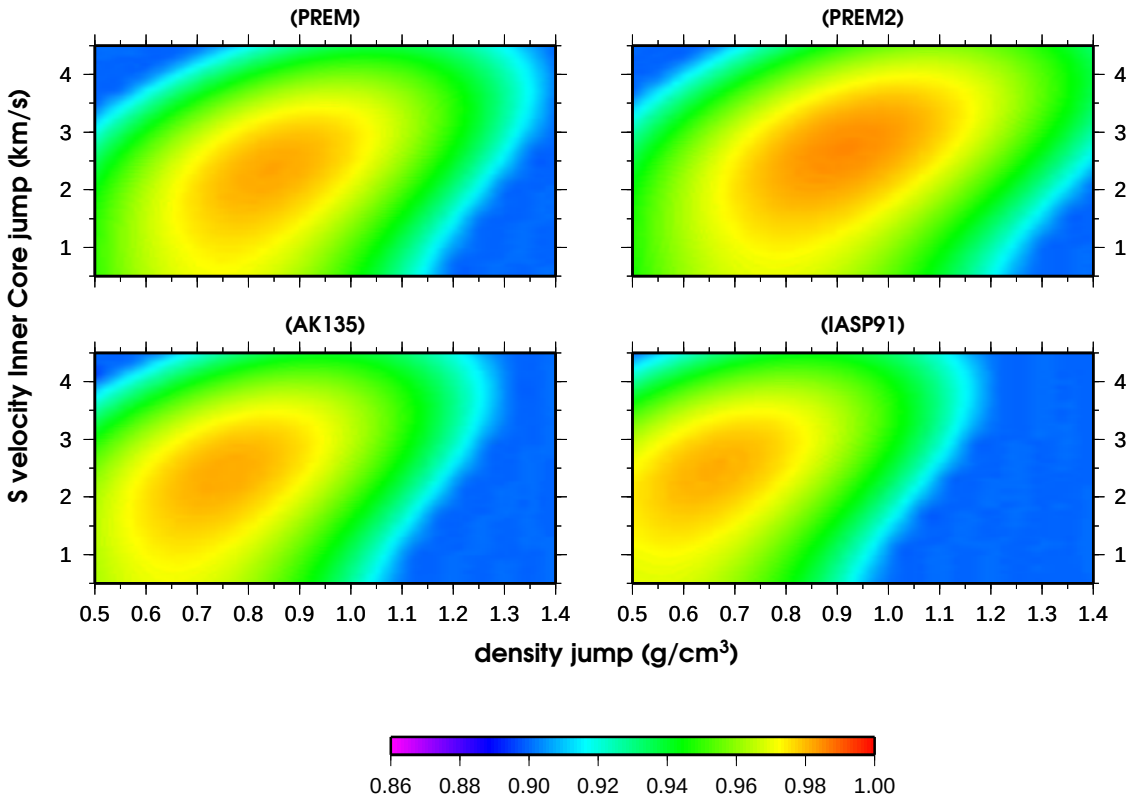

Figure 4: Variance reduction with respect to PREM (Dziewonski and Anderson, 1981), PREM2 (Song and Helmberger, 1995), IASP91 (Kennett and Engdahl, 1991), and AK135 (Kennett et al., 1995). The best fitting $\Delta\rho_{ICB}$ and $\Delta\beta_{ICB}are\sim$ $0.85gcm^{-3}$ and $\sim$2.5 kms^{-1}, $\sim$ $0.91gcm^{-3}$ and $\sim$ $2.6kms^{-1}$, $\sim$ $0.65gcm^{-3}$ and $\sim$ $2.5kms^{-1}$, and $\sim$ $0.75gcm^{-3}$ and $\sim$ $2.4kms^{-1}$, respectively.

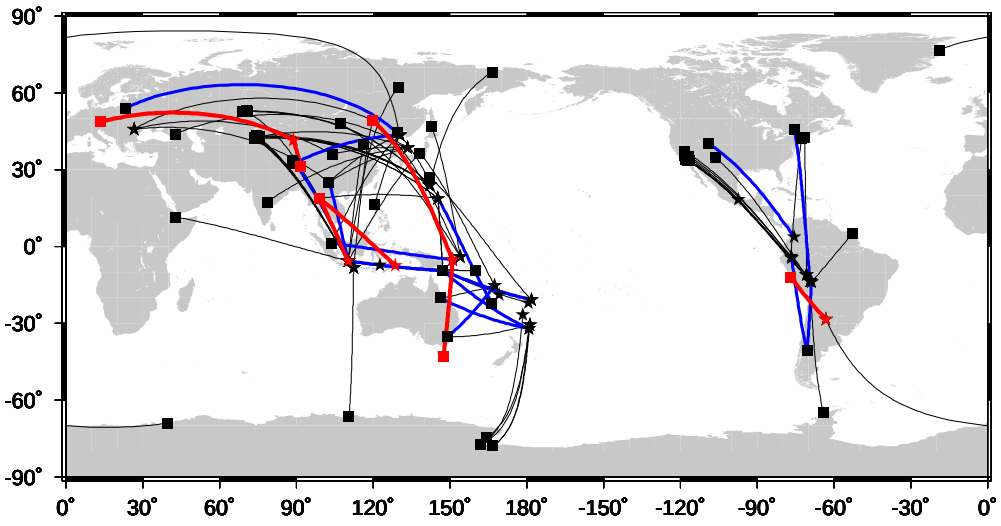

Figure 5: Geographical distribution of PKiKP and PcP ray paths. The red, blue, and black lines correspond to Quality A, A^-, and B subsets of data, respectively. The stars denote the events and the squares denote the stations.